Proceedings of the
44th IEEE Conference on Decision and Control, and
the European Control Conference 2005
Seville, Spain, December 12-15, 2005

On a Robust Bounded Control Design of the Combined Wheel Slip for an Autonomous 4WS4WD Ground Vehicle

Shou-Tao Peng, Che-Chia Hsu and Chau-Chin Chang
Department of Mechanical Engineering,
Southern Taiwan University of Technology, Tainan, Taiwan, R.O.C.

Abstract

This study presents a robust bounded control that prevents wheel skidding for an autonomous 4WS4WD vehicle under uncertain tire/road condition and aerodynamic drag. Constraint on combined wheel slip is incorporated as a priori in design to prevent the skidding. A robust low-and-high gain technique is used to suppress the path-tracking error and to enhance the utilization of the limited wheel slip. Simulation shows that, under the uncertain tire/road condition and aerodynamic drag, the proposed control scheme can effectively limit the combined wheel slip and achieve the goal of path tracking. Moreover, the control inputs of wheel torque and wheel steering are coordinated well during the path tracking.

Keywords: Bounded control, autonomous control, automotive control, combined wheel slip constraint, singular perturbation theory.

1. Introduction

In this paper, we study an issue of guiding an autonomous vehicle to approach and track a reference path without wheel skidding, when uncertainties of tire/road condition and aerodynamic drag are taken into account. Wheel skidding incurs abnormal wear of tire and, in cases, can cause vehicles out of control. The wheel skidding is related to the magnitude of combined wheel slip [1]-[2]. When the magnitude of combined wheel slip exceeds the threshold associated with road condition, tire/road friction saturates and wheel skidding occurs. Conversely, when the magnitude of combined wheel slip is retained within the threshold, the skidding does not take place.

The combined wheel slip consists of two coupled components: namely, the longitudinal and lateral wheel slips. However for simplicity, most vehicle control designs separate these two components to independently develop the relevant controllers. And only few designs, later for integration, combine these independently developed controllers with modifications using the concept of friction circle (see [3]-[7] and references therein). As a result, the overall stability of the new combined system is not easily guaranteed and the coordination between wheel torque and wheel steering could not be well in response to the combined control.

Due to the locally fast and exponential convergence of the wheel subsystem to its quasi-steady state, Peng, *et al* [8] incorporate the combined wheel slip as a priori in the control design, and regard the quasi-steady state of the combined wheel slip as the constraint target to develop the anti-skidding controller. By the approach, the combined wheel slip can be effectively limited below a pre-specified constraint during the tracking control. However in their study, the influence of aerodynamic drag is not considered. It is known that aerodynamic drag is the main disturbance that reduces vehicle speed from its set point. Thus, it is an instability factor and needs to be coped with. This study follows the approach of reference [8] to prevent wheel skidding, and in addition, considers the uncertainties of tire/road condition and aerodynamic drag for developing the autonomous control. Based on the design model, a control structure of wheel torque and wheel steering is presented, and a low-and-high gain with robust compensation is introduced to attenuate the tracking error. Simulation shows that, under the uncertain tire/road condition and aerodynamic drag, the proposed control can achieve the goal of path tracking and effectively limit the combined wheel slip. Moreover, the control shows good coordination between the control inputs of wheel torque and wheel steering. The control not only provides differential wheel torque to improve cornering performance, but also yields driven wheel torque to retain vehicle speed from the aerodynamic drag.

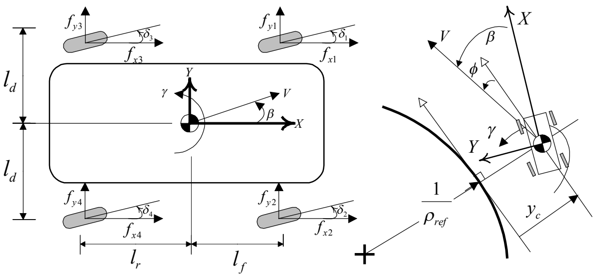

Figure 1. Vehicle system and tracking path

2 System Modeling

2.1 Vehicle system

As shown in Fig. 1, we consider a vehicle system that comprises three subsystems: namely, the vehicle body, four wheels, and kinematics between the vehicle and desired path. Variables for the vehicle body are the speed $v = \|V\|$ of center of gravity (CG), the sideslip angle β, and the yaw rate γ. Variables for the wheels are the wheel angular speeds ω_j ($j = 1,...,4$). Generalized coordinates describing the kinematics are the perpendicular distance y_c and the angle ϕ between the velocity V and the tangent to the path curve. The dynamical equations are expressed below [1],[2],[10]:

2.1.1 Vehicle body dynamics

$$\begin{bmatrix} m & 0 & 0 \\ 0 & mv & 0 \\ 0 & 0 & J_z \end{bmatrix} \frac{d}{dt} \begin{bmatrix} v \\ \beta \\ \gamma \end{bmatrix} = \begin{bmatrix} \cos\beta & \sin\beta & 0 \\ -\sin\beta & \cos\beta & 0 \\ 0 & 0 & 1 \end{bmatrix} \sum_{j=1}^{4} \begin{bmatrix} f_{xj} \\ f_{yj} \\ M_{zj} \end{bmatrix} + \begin{bmatrix} -\sigma_{aero} v^2 \cos\beta \\ \sigma_{aero} v^2 \sin\beta - mv\gamma \\ 0 \end{bmatrix} \quad (1a)$$

$$\sigma_{aero} = \rho_{air} C_{aero} A_f / 2 \quad (1b)$$

$$\begin{aligned} \textstyle\sum_{j=1}^{4} M_{zj} = {} & [-l_d \;\; l_f][f_{x1} \;\; f_{y1}]' + [l_d \;\; l_f][f_{x2} \;\; f_{y2}]' \\ & + [-l_d \;\; -l_r][f_{x3} \;\; f_{y3}]' + [l_d \;\; -l_r][f_{x4} \;\; f_{y4}]' \end{aligned} \quad (1c)$$

where ρ_{air}, C_{aero}, and A_f are respectively the air density, the coefficient of aerodynamic drag, and the front projection area of vehicle. f_{xj}, f_{yj}, and M_{zj} ($j = 1,..,4$), defined in the body-fixed $X-Y-Z$ coordinate, are the external forces and yaw moments mainly resulting from tire/road friction. Notations m and J_z are the mass of vehicle and the inertia about Z axis. Symbols l_f, l_r, and l_d are respectively the distances measured from the CG to the front, the rear axles, and to the wheel side.

0-7803-9568-9/05/$20.00 ©2005 IEEE

2.1.2 Wheel dynamics

$$I_{wj}\frac{d}{dt}\omega_j = T_j - r_{ej}\begin{bmatrix}\cos\delta_j & \sin\delta_j\end{bmatrix}\begin{bmatrix}f_{xj}\\ f_{yj}\end{bmatrix} \tag{2}$$

where I_{wj}, r_{ej} represent the inertia and the effective radius of wheel j; T_j, δ_j are the wheel torque and wheel steering angle used for control scheme.

2.1.3 Interaction between vehicle and reference path

Kinematics of the interaction can be expressed as [10]

$$\dot{y}_c = -v\sin\phi \tag{3a}$$

$$\dot{\phi} = -\frac{v}{(1/\rho_{ref}) + y_c}\cos\phi + \dot{\beta} + \gamma \tag{3b}$$

where the path curvature ρ_{ref}, assumed to be constant, is given.

2.1.4 Ranges of σ_{aero} and ρ_{ref}

In accordance with the changes of environment, we assume the coefficient σ_{aero} in Eq. (1b) varies in a known interval $\Omega_\sigma \subset \Re_+$ with

$$|\sigma_{aero} - \tilde{\sigma}_{aero}| \le \tilde{\mu}\tilde{\sigma}_{aero}, \quad \forall \sigma_{aero} \in \Omega_\sigma \tag{4}$$

where $\tilde{\sigma}_{aero}$ is the midpoint of the interval, and $\tilde{\mu} \ge 0$ is the normalized radius. We also assume the path curvature ρ_{ref} falls in a set $\Omega_\rho \subset \Re$ which contains all the curvatures of a standard road. In general, the curvatures of a standard road lie in a range of $[-1/400, 1/400]$ [3].

2.2 Calculation of friction force

To model the friction forces in Eq. (1), we need the following normal load transfer, combined wheel slip, and friction coefficient (see [2], [3], [7] and references therein).

2.2.1 Normal load transfer

The normal loads on the four wheels can be expressed as

$$f_{z1} = \frac{1}{2}\left(\frac{l_r mg - (h_{aero} - h) f_{aero}}{l_f + l_r} - \frac{h\sum_{j=1}^4 f_{xj}}{l_f + l_r} - \frac{k_{f\phi}(h/l_d)\sum_{j=1}^4 f_{yj}}{k_{f\phi} + k_{r\phi}}\right) \tag{5a}$$

$$f_{z2} = \frac{1}{2}\left(\frac{l_r mg - (h_{aero} - h) f_{aero}}{l_f + l_r} - \frac{h\sum_{j=1}^4 f_{xj}}{l_f + l_r} + \frac{k_{f\phi}(h/l_d)\sum_{j=1}^4 f_{yj}}{k_{f\phi} + k_{r\phi}}\right) \tag{5b}$$

$$f_{z3} = \frac{1}{2}\left(\frac{l_f mg + (h_{aero} - h) f_{aero}}{l_f + l_r} + \frac{h\sum_{j=1}^4 f_{xj}}{l_f + l_r} - \frac{k_{r\phi}(h/l_d)\sum_{j=1}^4 f_{yj}}{k_{f\phi} + k_{r\phi}}\right) \tag{5c}$$

$$f_{z4} = \frac{1}{2}\left(\frac{l_f mg + (h_{aero} - h) f_{aero}}{l_f + l_r} + \frac{h\sum_{j=1}^4 f_{xj}}{l_f + l_r} + \frac{k_{r\phi}(h/l_d)\sum_{j=1}^4 f_{yj}}{k_{f\phi} + k_{r\phi}}\right) \tag{5d}$$

In Eq. (5), $f_{aero} = \sigma_{aero}v^2$ is the aerodynamic drag force; h_{aero} is the height of the drag force acting on the vehicle body; h is the height of the CG; g is the gravitational constant; $k_{f\phi}$ and $k_{r\phi}$ are respectively the front and rear roll stiffness. For the normal loads (5), it is remarkable that the effect of the moment $(h_{aero} - h) f_{aero}$, arising from the drag force, is quite smaller than that of the moment $l_j mg$ resulting from the vehicle weight.

2.2.2 Combined Wheel slip

The combined wheel slip S_j of each wheel j is defined as

$$S_j = \begin{bmatrix} s_{Lj}\\ s_{Sj}\end{bmatrix} = \frac{1}{\max\left(r_{ej}\omega_j\cos\alpha_j, \|V_j\|\right)}\begin{bmatrix} r_{ej}\omega_j\cos\alpha_j - \|V_j\|\\ r_{ej}\omega_j\sin\alpha_j\end{bmatrix} \tag{6}$$

where V_j, α_j are respectively the wheel center velocity and slip angle given as

$$V_1 = \begin{bmatrix} v_{x1}\\ v_{y1}\end{bmatrix} = \begin{bmatrix} v\cos\beta - l_d\gamma\\ v\sin\beta + l_f\gamma\end{bmatrix}, \quad V_2 = \begin{bmatrix} v_{x2}\\ v_{y2}\end{bmatrix} = \begin{bmatrix} v\cos\beta + l_d\gamma\\ v\sin\beta + l_f\gamma\end{bmatrix}$$

$$V_3 = \begin{bmatrix} v_{x3}\\ v_{y3}\end{bmatrix} = \begin{bmatrix} v\cos\beta - l_d\gamma\\ v\sin\beta - l_r\gamma\end{bmatrix}, \quad V_4 = \begin{bmatrix} v_{x4}\\ v_{y4}\end{bmatrix} = \begin{bmatrix} v\cos\beta + l_d\gamma\\ v\sin\beta - l_r\gamma\end{bmatrix}$$

$$\alpha_j = \delta_j - \beta_j, \quad \beta_j = \tan^{-1}(v_{yj}/v_{xj}), \quad j = 1, \ldots, 4$$

2.2.3 Friction coefficient and force

The friction force of wheel j is given as

$$\begin{bmatrix} f_{xj} & f_{yj}\end{bmatrix}' = f_{zj}\begin{bmatrix}\mu_{xj} & \mu_{yj}\end{bmatrix}' \tag{7}$$

where f_{zj} is normal load (5), and (μ_{xj}, μ_{yj}) is friction coefficient obtained by using Eq. (6) with the following coordinate transform

$$\begin{bmatrix}\mu_{xj}\\ \mu_{yj}\end{bmatrix} = \begin{bmatrix}\cos\beta_j & -\sin\beta_j\\ \sin\beta_j & \cos\beta_j\end{bmatrix}\begin{bmatrix}1 & 0\\ 0 & k_{sj}\end{bmatrix}\frac{\mu_{\mathrm{Res}}\left(\|S_j\|, \chi\right)}{\|S_j\|}S_j \tag{8}$$

In Eq. (8), $k_{sj} \in [0.9,\ 0.95]$ is an attenuation factor used when tire tread profile is present. μ_{Res} is a scalar saturation function depending on the magnitude of combined wheel slip $\|S_j\|$ and road condition χ [2]. It is known that when $\|S_j\|$ exceeds a threshold associated with road condition, the corresponding μ_{Res} saturates and so does the related friction force (7). Conversely, the saturation of friction force can be avoided, provided $\|S_j\|$ is limited below the related threshold. For each road condition χ, it is commonly assumed that

(a) $\mu_{\mathrm{Res}}(0, \chi) = 0$

(b) $$k_j \triangleq \left.\frac{\partial\mu_{\mathrm{Res}}\left(\|S_j\|, \chi\right)}{\partial\|S_j\|}\right|_{\|S_j\| = 0} = \lim_{\|S_j\| \to 0_+}\frac{\mu_{\mathrm{Res}}\left(\|S_j\|, \chi\right)}{\|S_j\|} \tag{9}$$

The initial slope k_j in Eq. (9) depends mainly on road conditions. A better road condition gives a larger slope k_j and in turn provides a larger friction coefficient.

3 Linear design model and assumptions

3.1 Linearization with order reduction

We neglect the effect of the moment $(h_{aero} - h) f_{aero}$ in Eq. (5) and linearize the vehicle system around the operating point:

$$\rho_{ref,0} = 0, \|V_0\| = v_0, \beta_0 = 0, \gamma_0 = 0, w_{j0} = v_0/r_{ej},$$
$$y_{c0} = 0, \phi_0 = 0, \delta_{j0} = 0, T_{j0} = 0, \quad j = 1, \ldots, 4. \tag{10}$$

Using vehicle data [1] to characterize the linearization shows that the linearized wheel subsystem converges much faster and exponentially to its quasi-steady state below [8]

$$\partial\omega_j = \frac{1}{r_{ej}}\left(\partial v + (-1)^j\gamma l_d\right) + \frac{v_0}{r_{ej}^2 k_j f_{zsj}}T_j \tag{11}$$

with $\partial v \triangleq v - v_0$, $\partial\omega_j \triangleq \omega_j - \omega_{j0}$. Thus based on singular perturbation theory for order reduction, we replace the linearized wheel subsystem with its quasi-steady state (11), and finally arrive at the following design model:

(a) The linearized vehicle system:

$$\frac{d}{dt}\begin{bmatrix}\partial v\\ \beta\\ \gamma\\ y_c\\ \phi\end{bmatrix} = \begin{bmatrix} -2\sigma_{aero}v_0/m & 0 & 0 & 0 & 0\\ 0 & \sigma_{aero}v_0/m & -1 & 0 & 0\\ 0 & 0 & 0 & 0 & 0\\ 0 & 0 & 0 & 0 & -v_0\\ 0 & \sigma_{aero}v_0/m & 0 & 0 & 0\end{bmatrix}\begin{bmatrix}\partial v\\ \beta\\ \gamma\\ y_c\\ \phi\end{bmatrix} + \begin{bmatrix} 1/m & 0 & 0\\ 0 & 1/mv_0 & 0\\ 0 & 0 & 1/J_z\\ 0 & 0 & 0\\ 0 & 1/mv_0 & 0\end{bmatrix}\sum_{j=1}^4\begin{bmatrix} f_{xj}\\ f_{yj}\\ M_{zj}\end{bmatrix} + \begin{bmatrix} -\sigma_{aero}v_0^2/m\\ 0\\ 0\\ 0\\ -v_o\rho_{ref}\end{bmatrix} \tag{12}$$

(b) The simplified tire/road friction model (f_{xj}, f_{yj}, M_{zj}) **:**

Using replacement (11), the friction (f_{xj}, f_{yj}, M_{zj}) in Eq. (12) can be expressed using the following cascade form:

- *From the control input* (T_j, δ_j) *to the following quasi-steady-state wheel slip* $\tilde{S}_j$ *.*

$$\tilde{S}_1 = \begin{bmatrix} \dfrac{T_1}{r_{e1} f_{zs1} k_1} \\ -\beta - \dfrac{l_f \gamma}{v_0} + \delta_1 \end{bmatrix}, \tilde{S}_2 = \begin{bmatrix} \dfrac{T_2}{r_{e2} f_{zs2} k_2} \\ -\beta - \dfrac{l_f \gamma}{v_0} + \delta_2 \end{bmatrix}, \tilde{S}_3 = \begin{bmatrix} \dfrac{T_3}{r_{e3} f_{zs3} k_3} \\ -\beta + \dfrac{l_r \gamma}{v_0} + \delta_3 \end{bmatrix}, \tilde{S}_4 = \begin{bmatrix} \dfrac{T_4}{r_{e4} f_{zs4} k_4} \\ -\beta + \dfrac{l_r \gamma}{v_0} + \delta_4 \end{bmatrix} \tag{13}$$

- *From the quasi-steady-state wheel slip* $\tilde{S}_j$ *to the following friction output* (f_{xj}, f_{yj}, M_{zj})*:*

$$\begin{bmatrix} f_{x1} \\ f_{y1} \\ M_{z1} \end{bmatrix} = \begin{bmatrix} 1 & 0 \\ 0 & 1 \\ -l_d & l_f \end{bmatrix} \begin{bmatrix} f_{zs1} k_1 & 0 \\ 0 & k_{s1} f_{zs1} k_1 \end{bmatrix} \tilde{S}_1, \quad \begin{bmatrix} f_{x2} \\ f_{y2} \\ M_{z2} \end{bmatrix} = \begin{bmatrix} 1 & 0 \\ 0 & 1 \\ l_d & l_f \end{bmatrix} \begin{bmatrix} f_{zs2} k_2 & 0 \\ 0 & k_{s2} f_{zs2} k_2 \end{bmatrix} \tilde{S}_2,$$

$$\begin{bmatrix} f_{x3} \\ f_{y3} \\ M_{z3} \end{bmatrix} = \begin{bmatrix} 1 & 0 \\ 0 & 1 \\ -l_d & -l_r \end{bmatrix} \begin{bmatrix} f_{zs3} k_3 & 0 \\ 0 & k_{s3} f_{zs3} k_3 \end{bmatrix} \tilde{S}_3, \quad \begin{bmatrix} f_{x4} \\ f_{y4} \\ M_{z4} \end{bmatrix} = \begin{bmatrix} 1 & 0 \\ 0 & 1 \\ l_d & -l_r \end{bmatrix} \begin{bmatrix} f_{zs4} k_4 & 0 \\ 0 & k_{s4} f_{zs4} k_4 \end{bmatrix} \tilde{S}_4, \tag{14}$$

In Eq. (14), k_{sj} and k_j are defined in Eqs. (8) and (9); f_{zsj} are the static normal loads on the four wheels, defined as

$$\begin{bmatrix} f_{zs1} & f_{zs2} & f_{zs3} & f_{zs4} \end{bmatrix}' = \frac{mg}{2} \begin{bmatrix} \dfrac{l_r}{l_f + l_r} & \dfrac{l_r}{l_f + l_r} & \dfrac{l_f}{l_f + l_r} & \dfrac{l_f}{l_f + l_r} \end{bmatrix}' \tag{15}$$

In other words, when the vehicle system operates around condition (10), the combination of wheel subsystem (2) and tire/road friction (5)-(8) can be regarded as the actuator, of which the BIBO stable and comparatively faster dynamics is neglected and replaced by the related quasi-steady state instead. Also notice that if substituting Eqs. (13)-(15) into vehicle system (12), the resulting system takes a subsystem (β, γ) identical to the linear two-track mode commonly used in literature.

3.2 System assumptions

Some assumptions are given as follows:

Assumption 1. All the wheels have the same effective radius r_e and attenuation factor k_s. Hence in Eqs. (13) and (14), we have $r_{ej} = r_e$, $k_{sj} = k_s$, $j = 1,...,4$.

Assumption 2. The vehicle runs on a uniform road condition. More specially, the initial slopes (9) have the same value as k. Hence in Eqs. (13) and (14), we have $k_j = k$, $j = 1,...,4$.

Assumption 3. The wheel subsystem starts close to its quasi-steady state.

We also assume that the exact value of the above tire/road parameter (r_e, k_s, k) is not known, and only the estimated value $(\tilde{r}_e, \tilde{k}_s, \tilde{k})$ is used to construct the proposed control.

Suppose the design model (12)-(15) can be stabilized by the control input (T_j, δ_j) with state feedback; and meanwhile, the magnitude of $\tilde{S}_j$ is ensured below a pre-specified constraint s_c. Then, the original high order nonlinear vehicle system can also be locally stabilized around the operating point (10) using the same control scheme, since Jacobian linearization plus singular perturbation theory ensures the local stability can be concluded by using the stability of the reduced (slow) system [9]. Moreover, the magnitude of wheel slip S_j can be limited approximately below the constraint s_c, it is because singular perturbation theory guarantees that trajectories of a fast and BIBO stable subsystem can remain within an $O(\varepsilon)$ neighborhood of the quasi-steady state, if the trajectories start in the $O(\varepsilon)$ neighborhood [9]. Hence in the following sections, we will present a (T_j, δ_j) control scheme to achieve the concept.

4 Controller design

4.1 Control objective

For guiding a vehicle to approach and track a reference path of curvature $\rho_{ref} \in \Omega_\rho$ in a constant speed v_0, we choose the following state

$$x_d = \begin{bmatrix} \partial v_d & \beta_d & \gamma_d & y_{c,d} & \phi_d \end{bmatrix}' = \begin{bmatrix} 0 & 0 & v_0 \rho_{ref} & 0 & 0 \end{bmatrix}' \tag{16}$$

as the set point. Under uncertain tire/road condition (r_e, k_s, k) and uncertain coefficient of aerodynamic drag $\sigma_{aero} \in \Omega_\sigma$, the control objective is two-fold: one is to achieve state regulation (16), and the other is to limit the magnitude of quasi-steady-state wheel slip $\tilde{S}_j$ below a pre-specified value s_c.

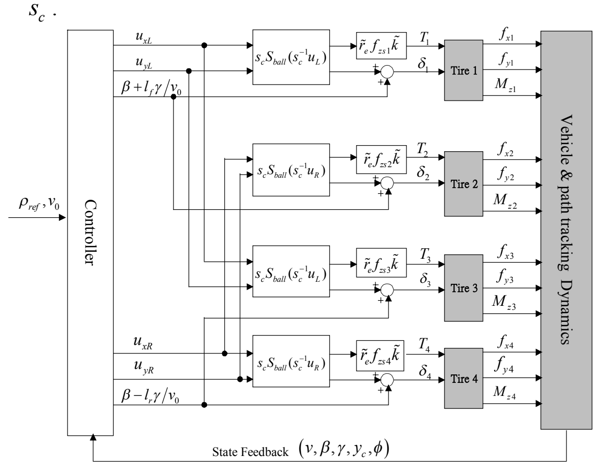

Figure 2. An illustration of the control structure

4.2 Control structure of wheel torque and wheel steering

Let $(\tilde{r}_e, \tilde{k}_s, \tilde{k}, \tilde{\sigma}_{aero})$ be the estimated values of $(r_e, k_s, k, \sigma_{aero})$. Define a unit-ball saturation function $S_{ball} : \Re^2 \to \Re^2$ as

$$S_{ball}(z) = \begin{cases} z, & \|z\| \le 1 \\ z / \|z\|, & \|z\| > 1 \end{cases}, z \in \Re^2 \tag{17}$$

As shown in Fig.2, the control structure of wheel torque and wheel steering is given as [8]:

$$\begin{bmatrix} T_j \\ \delta_j \end{bmatrix} = \begin{bmatrix} \tilde{r}_e f_{zsj} \tilde{k} & 0 \\ 0 & 1 \end{bmatrix} \left(\begin{bmatrix} 0 \\ \beta + l_j \gamma / v_0 \end{bmatrix} + s_c S_{ball} \left(s_c^{-1} u_j \right) \right) \tag{18a}$$

$$l_1 = l_2 = l_f, \; l_3 = l_4 = -l_r, \; u_1 = u_3 = u_L, \; u_2 = u_4 = u_R \tag{18b}$$

where f_{zsj} is static normal load (15), and (u_L, u_R) is the bounded controller to be defined in the next section.

Substituting control structure（18）into design model (12)-(15), with Assumptions 1 and 2, gives

$$\dot{x} = (A+\Delta_a)x + B(I_4+\Delta_b)\begin{bmatrix} S_{ball}(s_c^{-1}u_L) \\ S_{ball}(s_c^{-1}u_R) \end{bmatrix} + d \tag{19}$$

where I_4 is a 4×4 identity matrix and $x=\left[\partial v \;\; \beta \;\; \gamma \;\; y_c \;\; \phi\right]'$, $d=\left[-\sigma_{aero}v_0^2/m \;\; 0 \;\; 0 \;\; 0 \;\; -v_o\rho_{ref}\right]'$,

$$A=\begin{bmatrix} -2\tilde{\sigma}_{aero}v_0/m & 0 & 0 & 0 & 0 \\ 0 & \tilde{\sigma}_{aero}v_0/m & -1 & 0 & 0 \\ 0 & 0 & 0 & 0 & 0 \\ 0 & 0 & 0 & 0 & -v_0 \\ 0 & \tilde{\sigma}_{aero}v_0/m & 0 & 0 & 0 \end{bmatrix},$$

$$B=s_c\begin{bmatrix} (f_{zs1}+f_{zs3})\tilde{k}/m & 0 & (f_{zs2}+f_{zs4})\tilde{k}/m & 0 \\ 0 & \tilde{k}_s(f_{zs1}+f_{zs3})\tilde{k}/mv_0 & 0 & \tilde{k}_s(f_{zs2}+f_{zs4})\tilde{k}/mv_0 \\ -l_d(f_{zs1}+f_{zs3})\tilde{k}/J_z & 0 & l_d(f_{zs2}+f_{zs4})\tilde{k}/J_z & 0 \\ 0 & 0 & 0 & 0 \\ 0 & \tilde{k}_s(f_{zs1}+f_{zs3})\tilde{k}/mv_0 & 0 & \tilde{k}_s(f_{zs2}+f_{zs4})\tilde{k}/mv_0 \end{bmatrix},$$

$$\Delta_a=\frac{(\sigma_{aero}-\tilde{\sigma}_{aero})v_0}{m}\begin{bmatrix} -2 & 0 & 0 & 0 & 0 \\ 0 & 1 & 0 & 0 & 0 \\ 0 & 0 & 0 & 0 & 0 \\ 0 & 0 & 0 & 0 & 0 \\ 0 & 1 & 0 & 0 & 0 \end{bmatrix},$$

$$\Delta_b=diag\left((\tilde{r}_e-r_e)/r_e,\ \left(k_sk-\tilde{k}_s\tilde{k}\right)/\tilde{k}_s\tilde{k},\ (\tilde{r}_e-r_e)/r_e,\ \left(k_sk-\tilde{k}_s\tilde{k}\right)/\tilde{k}_s\tilde{k}\right)$$

In system（19）, the uncertainties Δ_a and Δ_b respectively reflect the mismatching between the estimated and the exact values of the aerodynamic coefficient and those of the tire/road data. The disturbance d arises from the influences of the aerodynamic drag, tracking curvature, and tracking speed. Some properties of control structure (18) and system (19) are summarized as follows:

(I) Property of control structure (18)

(P1) *The control (18) is a decoupling scheme, and manipulating the term* $s_cS_{ball}(s_c^{-1}u_j)$ *inside it can be interpreted as manipulating the quasi-steady-state wheel slip* $\tilde{S}_j$ *inside friction model (13)-(15).*

This approximation $\tilde{S}_j \approx s_cS_{ball}(s_c^{-1}u_j)$ can be observed by substituting Eq. (18) into Eq. (13) with $\tilde{r}_e\tilde{k} \approx r_{ej}k_j = r_ek$. And if $\tilde{r}_e\tilde{k} \le r_ek$ in particular, then the constraint objective $\left\|\tilde{S}_j\right\| \le s_c$ is achieved. Moreover, The arrangement of structure (18) can be used to cope with the μ-split road condition [8] (i.e., a road condition which has different surface properties on the left and right sides).

(II)Property of system（19）

(P2) *The pair* (A,B) *is controllable.*

(P3) *Concerning the uncertainty* Δ_a: For set point (16),

$$\Delta_ax_d = 0_{5\times 1} \tag{20}$$

Moreover from inequality (4), the following matrix

$$\tilde{D}=\frac{\tilde{\mu}\tilde{\sigma}_{aero}v_0}{m}\begin{bmatrix} -2 & 0 & 0 & 0 & 0 \\ 0 & 1 & 0 & 0 & 0 \\ 0 & 0 & 0 & 0 & 0 \\ 0 & 0 & 0 & 0 & 0 \\ 0 & 1 & 0 & 0 & 0 \end{bmatrix}$$

satisfies

$$\Delta_a'\Delta_a \le \tilde{D}'\tilde{D},\ \ \forall \sigma_{aero}\in\Omega_\sigma \tag{21}$$

(P4) *Concerning the uncertainty* Δ_b: The uncertainty Δ_b satisfies

$$\Delta_b = \Delta_b' \ge 0_{4\times 4}$$

provided that the estimated parameter $(\tilde{r}_e,\tilde{k}_s,\tilde{k})$ is chosen with

$$\tilde{r}_e \ge r_e,\ \ \tilde{k}_s\tilde{k} \le k_sk\,.$$

(P5) *Concerning the disturbance* d*:* The matrix equation

$$Ax_d + B\Gamma + d = 0_{5\times 1} \tag{22}$$

has a solution

$$\Gamma=\begin{bmatrix} \dfrac{\sigma_{aero}v_0^2}{\sum_{j=1}^4 f_{zsj}\tilde{k}s_c} & \dfrac{mv_0^2\rho_{ref}}{\sum_{j=1}^4 f_{zsj}\tilde{k}_s\tilde{k}s_c} & \dfrac{\sigma_{aero}v_0^2}{\sum_{j=1}^4 f_{zsj}\tilde{k}s_c} & \dfrac{mv_0^2\rho_{ref}}{\sum_{j=1}^4 f_{zsj}\tilde{k}_s\tilde{k}s_c} \end{bmatrix}' \tag{23}$$

Consider a vector function $\Xi\left(\tilde{S}_j\right) \triangleq \sum_{j=1}^4\left[f_{xj}\;\; f_{yj}\right]'$ defined by summing the terms in Eq. (14) with (k_{sj},k_j) being replaced by $(\tilde{k}_s,\tilde{k})$. By mapping all elements in the four sets $\left\|\tilde{S}_j\right\| \le s_c$ through this *surjective* function $\Xi\left(\tilde{S}_j\right)$, Fig. 3 depicts the resulting projection, which can be verified as an elliptic shape taking semi-axes $a=\sum_{j=1}^4 f_{zsj}\tilde{k}s_c$ and $b=\sum_{j=1}^4 f_{zsj}\tilde{k}_s\tilde{k}s_c$. In this figure, the aerodynamic drag $\sigma_{aero}v_0^2$, centrifugal force $mv_0^2\rho_{ref}$, and their resultant force η are also plotted.

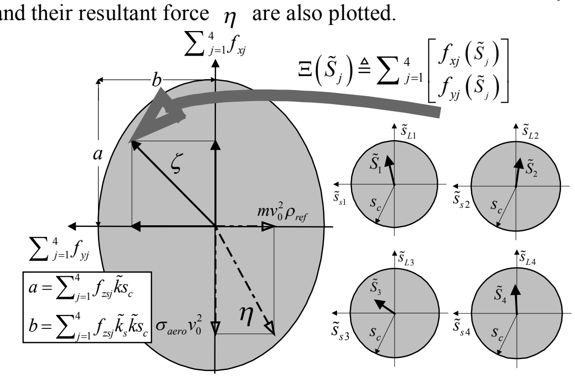

Figure 3. Friction circle subject to wheel slip constraint

As subjected to the wheel slip constraint s_c, this friction ellipse illustrates the ranges of all the possible estimated longitudinal and lateral tire/road friction forces (i.e., $\sum_{j=1}^4 f_{xj}$ and $\sum_{j=1}^4 f_{yj}$) and their resultant ζ. Obviously, for achieving the path tracking under the wheel slip constraint, the limited friction force must be able to conquer the external force η that vehicles encounter during the tracking. That is to say, the external force η must lie inside this friction ellipse. And more specifically, there exists $0 \le \tilde{\delta} < 1$ such that

$$\left(\frac{\sigma_{aero}v_0^2}{\sum_{j=1}^4 f_{zsj}\tilde{k}s_c}\right)^2 + \left(\frac{mv_0^2\rho_{ref}}{\sum_{j=1}^4 f_{zsj}\tilde{k}_s\tilde{k}s_c}\right)^2 \le \tilde{\delta}^2 < 1, \qquad \forall(\sigma_{aero},\rho_{ref})\in\Omega_\sigma\times\Omega_\rho \tag{24}$$

Assumption 4 below gives an equivalent statement of Eq. (24).

Assumption 4. There exists $0 \le \tilde{\delta} < 1$ such that the matrix Γ in Eq. (23) satisfies

$$\underset{(\sigma_{aero},\rho_{ref})\in\Omega_\sigma\times\Omega_\rho}{Max}\left\{\ \left\|E_1\Gamma\right\|\ ,\ \left\|E_2\Gamma\right\|\ \right\} \le \tilde{\delta} < 1 \tag{25}$$

with $E_1 \triangleq \left[I_2 \;\; 0_{2\times 2}\right]$, $E_2 \triangleq \left[0_{2\times 2} \;\; I_2\right]$ (26)

4.3 Robust bounded controller design

For set point (16), define regulation error as

$$e = x - x_d \tag{27}$$

By using system (19), Eqs. (20) and (22), the dynamical error equation can be obtained as

$$\dot{e} = (A + \Delta_a)e + B(I_4 + \Delta_b)\begin{bmatrix} S_{ball}(s_c^{-1}u_L) \\ S_{ball}(s_c^{-1}u_R) \end{bmatrix} - B\Gamma \tag{28}$$

Accordingly, the bounded controller (u_L, u_R) is proposed as

$$\begin{cases} u_L = -s_c\left(1+\gamma_H\right)E_1 B' P_\varepsilon e \\ u_R = -s_c\left(1+\gamma_H\right)E_2 B' P_\varepsilon e \end{cases} \tag{29}$$

where $P_\varepsilon = P_\varepsilon' > 0_{5\times 5}$ and $\gamma_H > 0$ are deign parameters. The matrix P_ε is a solution of the Riccati matrix inequality

$$(A+\Delta_a)'P_\varepsilon + P_\varepsilon(A+\Delta_a) - P_\varepsilon BB'P_\varepsilon + \varepsilon I_5 \le 0_{5\times 5}, \forall \sigma_{aero} \in \Omega_\sigma$$

with $\varepsilon > 0$ being sufficiently small. Or sufficiently by using matrix inequality (21), the matrix P_ε can be chosen as a solution of the following algebraic Riccati equation (ARE) [6]

$$A'P_\varepsilon + P_\varepsilon A - P_\varepsilon(BB' - \tilde{h}_1^{-2}I_5)P_\varepsilon + \tilde{h}_1^2 \tilde{D}'\tilde{D} + \varepsilon I_5 = 0_{5\times 5} \tag{30}$$

with $\varepsilon > 0$ being sufficiently small and $h_1 > 0$. As $(h_1, \varepsilon, P_\varepsilon)$ is selected and fixed, the parameter γ_H must be set sufficiently large to satisfy the linear matrix inequality (LMI) below：

$$\frac{\tilde{\delta}^2}{\tilde{h}_2\sqrt{\gamma_H}} P_\varepsilon < \varepsilon I_5 + P_\varepsilon BB'P_\varepsilon, \ \frac{\tilde{h}_2}{\sqrt{\gamma_H}} < \frac{(1-\tilde{\delta})^2}{\lambda_{\max}(B'P_\varepsilon B)} \tag{31}$$

where $\tilde{h}_2 > 0$ is an auxiliary parameter for tuning γ_H. LMI (31) is always satisfied, because its right hand side is fixed, while its left hand side can be arbitrarily small as enlarging γ_H. Choosing $(\varepsilon, P_\varepsilon, \gamma_H)$ in the above manner is known as a low-and-high gain technique developed for bounded input control [12]-[13]. By this technique, utilization of the constrained control (i.e., the constrained wheel slip in this study) can be enhanced to robustly attenuate the tracking error (27).

4.4 Stability analysis

Consider a suitable solution $(\varepsilon, \tilde{h}_1, P_\varepsilon, \gamma_H, \tilde{h}_2)$ chosen from ARE (30) and LMI (31). Let $V(e) = e'P_\varepsilon e$ be the Lyapunov function candidate. Then, the Lyapunov derivative of system (28) under control (29) can be expressed as

$$\dot{V}(e) = e'\left((A+\Delta_a)'P_\varepsilon + P_\varepsilon(A+\Delta_a)\right)e + 2e'P_\varepsilon B\begin{bmatrix} S_{ball}\left(-(1+\gamma_H)E_1B'P_\varepsilon e\right) \\ S_{ball}\left(-(1+\gamma_H)E_2B'P_\varepsilon e\right)\end{bmatrix}$$

$$-2e'P_\varepsilon B\Gamma + 2e'P_\varepsilon B\Delta_b \begin{bmatrix} S_{ball}\left(-(1+\gamma_H)E_1B'P_\varepsilon e\right) \\ S_{ball}\left(-(1+\gamma_H)E_2B'P_\varepsilon e\right)\end{bmatrix} \tag{32}$$

Theorem 1 below summaries the main result in this study.

Theorem 1. *Let Assumptions (1)-(4) hold. Then, with the solution* $(\varepsilon, \tilde{h}_1, P_\varepsilon, \gamma_H, \tilde{h}_2)$, *Lyapunov derivative (32) can be estimated as*

(1) $\dot{V}(e) < 0$, $\forall e \in \left\{e \in \Re^5 : c_1 < e'P_\varepsilon e < c_2\right\}$,

$c_1 \triangleq \tilde{h}_2 \big/ \sqrt{\gamma_H}$, $c_2 \triangleq (1-\tilde{\delta})^2 \big/ \lambda_{\max}(B'P_\varepsilon B)$.

Moreover,

(2) $\gamma_H \to \infty_+ \Rightarrow c_1 \to 0_+$

Proof. Omitted for brevity.

Based on practical stability [10], Theorem 1 indicates that feedback system (28)-(29) has a region of positive invariance $L_V(c_2) \triangleq \left\{e \in \Re^5 : e'P_\varepsilon e < c_2\right\}$ and a region of ultimate boundedness $L_V(c_1) \triangleq \left\{e \in \Re^5 : e'P_\varepsilon e \le c_1\right\}$. Moreover, the region $L_V(c_1)$ can be set arbitrarily small, provided γ_H is chosen sufficiently large. Accordingly, there exists a finite time $t_1 \ge 0$ such that

$$\forall e(0) \in L_V(c_2) \Rightarrow e(t) \in L_V(c_2), \forall t \ge 0 \Rightarrow e(t) \in L_V(c_1), \forall t \ge t_1.$$

Finally, by substituting controller (29) into control structure (18), we accomplish the robust bounded control design.

5 Simulations

The nonlinear vehicle model in section 2 is used for simulation. The desired travel speed is set as $v_0 = 25\,\mathrm{m/sec}$; and the desired path, covered with wet asphalt, is a circular path of curvature $\rho_{ref} = 1/400\,\mathrm{m}^{-1}$. The data of the vehicle system is given as: $\rho_{air} = 1.225$, $C_{aero} = 0.335$, $A_f = 1.824$, $h_{aero} = 0.57$, $m = 1480$, $J_z = 1950$, $l_f = 1.421$, $l_r = 1.029$, $l_d = 0.751$, $h = 0.42$, $k_{f\phi} = 50539$, $k_{r\phi} = 20972$, $r_{ej} = 0.31$, $I_{wj} = 0.7$, $k_s = 0.9$, $g = 9.81$.

The estimated parameters are set as $s_c = 0.05$, $\tilde{\sigma}_{aero} = 0.44$, $\tilde{\mu} = 0.16$, $\tilde{r}_e = 0.34$, $\tilde{k}_s = 0.85$, and $\tilde{k} = 12$. By using these estimated parameters, properties (P1), (P4), and inequality (21) are true. Besides, inequality (25) can be verified with $\tilde{\delta} = 0.3144$. For constructing controller (29), we choose $\varepsilon = 1\times 10^{-4}$, $\tilde{h}_1 = 50$, $\gamma_H = 40$, $\tilde{h}_2 = 2$, and the related P_ε to solve both ARE (30) and LMI (31). The following initial conditions are given for the simulation: $v(0) = 25\,\mathrm{m/sec}$, $\beta(0) = 0$ deg, $\phi(0) = 0$ deg, $y_c(0) = 30\mathrm{m}$.

Figure 4 shows that, under the control scheme, the vehicle approaches the desired path gradually, and eventually vehicle path almost overlaps the desired path. Figures 5(a) and 5(b) respectively illustrate the magnitudes of combined wheel slip of the four wheels in the steady state and in the transient. We can see that these magnitudes are almost all constrained below the pre-specified constraint $s_c = 0.05$. Moreover in the transient, these magnitudes are all pushed to the allowed maximum to acquire a better lateral acceleration as shown in Fig. 5(c). Figure 5(d) displays the wheel normal loads with respect to time. Figures 6(a) to 6(f) illustrate respectively the time histories of the mass center speed, sideslip angle, yaw rate, distance offset, angle between path slope and vehicle speed, and wheel angular speeds. Time profiles of the wheel steering angles and wheel torques are shown in Figs. 7(a) and 7(b) respectively. We can observe that not only the differential but also the driven wheel torque are generated so that the cornering performance can be improved and the vehicle speed can be retained from the aerodynamic drag (see also vehicle speed and yaw rate in Figs. 6(a) and 6(c)).

6 Conclusions

In this study, we present an anti-skidding control for an autonomous 4WS4WD vehicle under uncertain tire/road condition and aerodynamic drag. The approach of constraining combined wheel slip is used to prevent the skidding. For developing the control scheme, the actual combined wheel slip is replaced by its quasi-steady state, and a robust low-and-high gain technique is introduced to construct the control. Simulation shows that the control scheme effectively limits the wheel slip and accomplishes the path-tracking work. In addition, the control inputs of wheel torque and wheel steering are coordinated well during the tracking control.

7 Acknowledgements

The authors are grateful to National Science Council of R.O.C. for supporting this research (NSC 93-2218-E-218-006).

References

1. Genta, G, Motor Vehicle Dynamics, World Scientific, Singapore, 1997.
2. Kiencke, U. and Nielsen, L., Automotive Control Systems,

Springer, Berlin, 2000.
3. Alleyn A., “A Comparison of Alternative Intervention Strategies for Unintended Roadway Departure Control,” Vehicle System Dynamics, 27, pp. 157-186, 1997.
4. Rajamani, R., Tan, H. S., Law, B. K., and Zhang, W. B., “Demonstration of Integrated Longitudinal and Lateral Control for the Operation of Automated Vehicles in Platoons”, IEEE transaction on control systems technology, 8(4), pp.695-708, 2000.
5. Guldner, J., Sienel, W., Tan, H. S., and Ackermann, J., “Robust Automatic Steering Control for Look-Down Reference Systems with Front and Rear Sensors,” IEEE transaction on control systems technology, 7(1), pp.2-11, 1999.
6. Jia, Y., “Robust control with decoupling performance for steering and traction of 4WS vehicles under velocity-varying motion”, IEEE transaction on control systems technology, 8(3), pp.554-569, 2000.
7. Nagai, M. Shino, M. and Gao, F., “Study on integrated control of active front steer angle and direct yaw moment,” JSAE Review, 23, pp.309-315, 2002.
8. Peng, S. T., Sheu, J. J., and Chang, C. C., “A Control Scheme for Automatic Path Tracking of Vehicles Subject to Wheel Slip Constraint,” Proceedings of the American Control Conference, pp. 804-809, 2004.
9. Khalil, H. K., 2002, Nonlinear Systems 3rd Edition, Prentice Hall, Upper Saddle River, NJ.
10. Ackermann, J. *Robust Control*, Springer-Verlag, London, 1993.
11. Wong, J.Y., Theory of Ground Vehicles, John Wiley & Sons, Inc, 2001.
12. Peng, S. T., “On a modification approach to a class of Lyapunov-based robust controllers subject to input constrain,” Journal of the Franklin Institute, Vol. 341(4), pp. 343~360, 2004.
13. Saberi, A., Z. Lin, and A.R. Teel, “Control of Linear Systems With Saturating Actuators,” *IEEE transaction on Automatic Control*, 41(3), pp. 368-378, 1996.

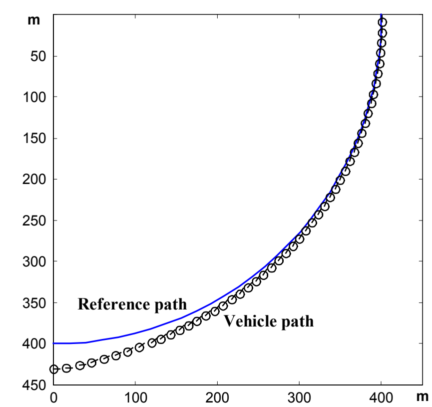

Figure 4

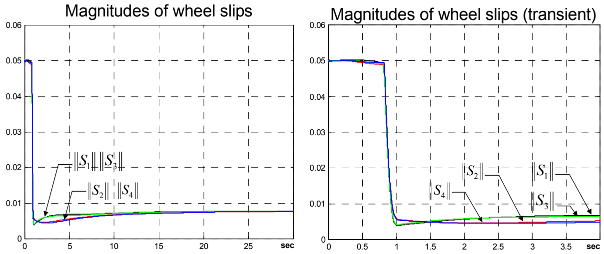

(a) (b)

Figure 5

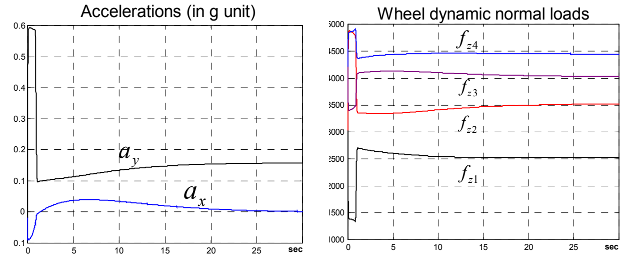

(c) Figure 5 (d)

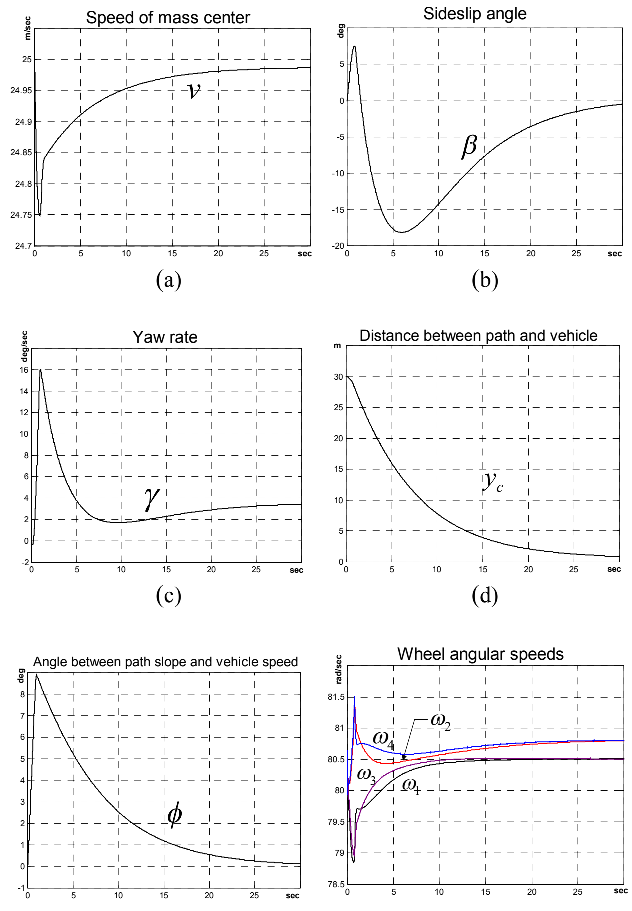

(a) (b)

(c) (d)

(e) (f)

Figure 6

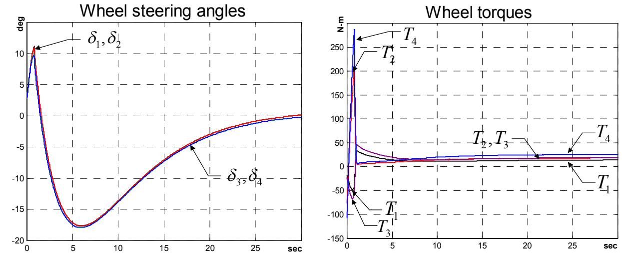

(a) (b)

Figure 7